Proceedings of the 11th ICPMG 2026
11th International Conference on Physical Modelling in Geotechnics
8-12 June 2026, Zurich, Switzerland

LEAP-Asia-2025 Centrifuge Experiments at Ehime University

K. Ono
Ehime University, Matsuyama City, Japan, ono.kohei.vb@ehime-u.ac.jp

T. Ogawa
Ehime University, Matsuyama City, Japan, n804005x@mails.cc.ehime-u.ac.jp

M. Okamura
Waseda University, Shinjuku-ku, Japan, m.okamura@waseda.jp

ABSTRACT: The Liquefaction Experiments and Analysis Project (LEAP) is an international collaborative initiative aimed at validating and quantifying uncertainties in centrifuge tests and numerical simulations related to soil liquefaction. The LEAP-Asia-2025 exercise focused on investigating the stability of a dam body constructed on potentially liquefiable foundation layers. This paper presents the results of four centrifuge tests conducted at Ehime University to evaluate experimental reproducibility and examine the influence of varying relative densities and centrifugal accelerations (*g*-levels). The paper details the construction of the liquefiable foundation and dam body, including sand placement techniques and saturation procedures. Furthermore, resistance profiles obtained from in-flight cone penetration tests are presented and compared with results from previous LEAP exercises. Typical experimental outputs—including excess pore water pressure response, acceleration time histories, and dam body deformation—are analysed. The results indicate that the deformation of the dam body was significantly influenced by the relative density of the foundation, whereas it remained relatively insensitive to the *g*-level.

1 INTRODUCTION

The Liquefaction Experiments and Analysis Project (LEAP) is an international collaborative initiative aimed at validating and quantifying uncertainties in centrifuge modelling and numerical simulations of soil liquefaction.

The first major exercise, LEAP-UCD-2017, focused on examining the repeatability, variability, and sensitivity of centrifuge tests in modelling lateral spreading in liquefiable soils (Kutter et al., 2020). A key lesson learned from these exercises is that centrifuge test results are significantly influenced by the initial conditions of the model and the specific experimental setup. Additionally, it was underscored that ensuring the repeatability of model tests is crucial for interpreting the variability observed in measurements and observations.

Building on these findings, LEAP-RPI-2020 and LEAP-GWU-2022 expanded the scope to more complex configurations, such as a uniform liquefiable sand layer supported by a sheet pile wall. Ono and Okamura (2024) summarized their efforts, emphasizing how variations in relative density and the intensity of input motions significantly affect the stability of the sheet pile.

The latest LEAP-Asia-2025 exercise focuses on investigating the stability of a dam body constructed on potentially liquefiable foundation layers. This paper presents the results of four centrifuge tests conducted at Ehime University to evaluate experimental reproducibility and examine the influence of varying relative densities and centrifugal accelerations (*g*-levels) on the stability of the dam body. Along with a detailed description of the experimental conditions and model preparation, typical experimental results are discussed, including excess pore water pressure response, acceleration time histories, and dam body deformation.

2 EXPERIMENT SETUP

2.1 Model specification

The dimensions, materials, and construction methods of the models complied with the specification (Ma et al., 2025). Figure 1 shows the schematic of the model. The internal dimensions of a rigid soil container are 510 × 120 × 230 mm (length × width × depth) in model scale. The rigid soil container with a transparent acrylic front panel was used, prioritizing the repeatability of model construction and the requirement for high-resolution image analysis of the deformation process. To minimize potential boundary effects such as the constraint of shear deformation, a dam body was positioned in the centre of the container, ensuring sufficient distance from the side walls.

The model consists of the dam body with a slope angle of 30 degrees, placed on a horizontal liquefiable foundation. In the specification, the prototype geometry of the liquefiable foundation is specified as 10 m thick, and the dam body is 5 m high. However, due to the constraints of the container size and centrifuge capacity, the model dimensions and centrifugal acceleration were adjusted so that the equivalent prototype dimensions would be 1/2 and 1/3 of the original specifications. Furthermore, the width of the soil container is approximately 1/4 of the specified dimension. Since the dimension in the width direction affects the frictional resistance from the walls (Wang et al., 2023), it may influence the deformation characteristics of the embankment. In this study, a total of four cases were conducted with identical model-scale dimensions but different relative densities of the foundation and different centrifugal accelerations (Table 1).

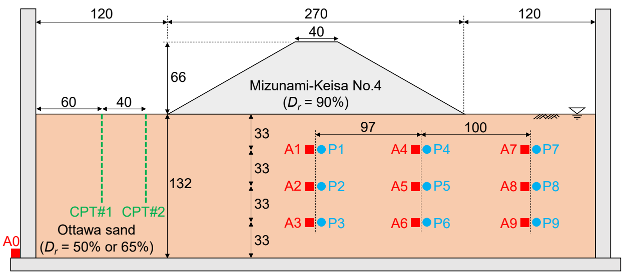

Figure 1. Model geometry and instrumentations (Dimensions in mm).

Table 1. Test cases.

Case ID	D_r of foundation before saturation (%)	Centrifugal acceleration (g)
DR50-38G	48.1	37.7
DR50-25G	46.1	25.2
DR65-38G	65.3	37.7
DR65-25G	62.6	25.2

2.2 Material

Ottawa F-65 sand was used as the material for the liquefiable foundation. The maximum and minimum dry densities of Ottawa sand are 1753 kg/m^3 and 1451 kg/m^3, respectively.

While all LEAP modelers use the same material for the foundation, only the grain size distribution is specified for the dam body material, leaving the specific selection to each institution. In this study, Mizunami-Keisa No. 4 was selected for the dam body. The sand is a coarse sand with a mean grain size of approximately 1 mm; its maximum and minimum dry densities are 1572 kg/m^3 and 1298 kg/m^3, respectively. Figure 2 shows the grain size distribution for each material.

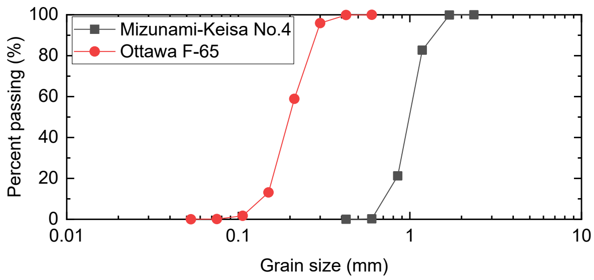

Figure 2. Grain size distribution.

2.3 Model construction

The foundation was prepared using the air pluviation method. The funnel openings were set to 2.5 mm for a relative density of 50% and 2.0 mm for 65%. The foundation was constructed in four layers, corresponding to the installation heights of the pore pressure transducers (P1 to P9) and accelerometers (A1 to A9) shown in Figure 1. The surface level of each layer was adjusted using a vacuum cleaner while carefully measuring the height with a laser displacement sensor.

Subsequently, the soil container was placed in a vacuum chamber, and a viscous fluid was permeated under a negative pressure of -95 kPa. The viscous fluid was prepared by dissolving methylcellulose in boiled tap water. After the saturation process, the degree of saturation was measured following the method described by Okamura and Inoue (2012).

The dam body was prepared by compacting the specimen, adjusted to a water content of 12%, to a relative density of 90% within a mould, followed by freezing. The frozen dam body was then removed from the mould and placed on the saturated foundation. Any gaps between the container walls and the dam body were filled with the same material as the dam body. After installation, the model was left for at least five hours until the dam body had completely thawed.

2.4 Experiment procedure

The beam-type centrifuge at Ehime University was used for the experiments. After reaching the target centrifugal acceleration (37.7 g or 25.2 g), cone penetration test (CPT) was conducted at the locations shown in Figure 1 to verify the density and vertical uniformity of the foundation. At the dam crest, slight settlements were measured during the increase of centrifugal acceleration, with maximum values of 0.8 mm and 0.5 mm in model scale for the cases with relative densities of 50% and 65%, respectively.

A miniature cone penetrometer with a diameter of 6 mm in the model scale (Carey et al. (2020)) was penetrated at a sufficiently low velocity of 0.7 mm/s to prevent the generation of excess pore water pressure during penetration.

Following the CPT, base shaking was applied while the centrifuge remained in operation. Figure 3 shows the time histories of acceleration and Arias Intensity, along with the 5% damped acceleration response spectra of the shaking table. Although the reference waveform for base shaking is defined in the specifications, it is difficult to perfectly replicate all parameters, including peak acceleration amplitude ($a_{\max} = 2.0$ m/s^2), period ($T = 1.0$ s), and duration ($D_{5\text{-}95} = 11.8$ s). Therefore, in this study, the input wave was pre-adjusted to match the specified Arias Intensity (I_a = 3.2 m/s) while using the peak acceleration amplitude as the primary benchmark. As shown in Figure 3, the obtained waveforms reasonably satisfied the criteria for $a_{\max}$, I_a, and T.

In the following sections, all results are presented in the prototype scale unless otherwise mentioned.

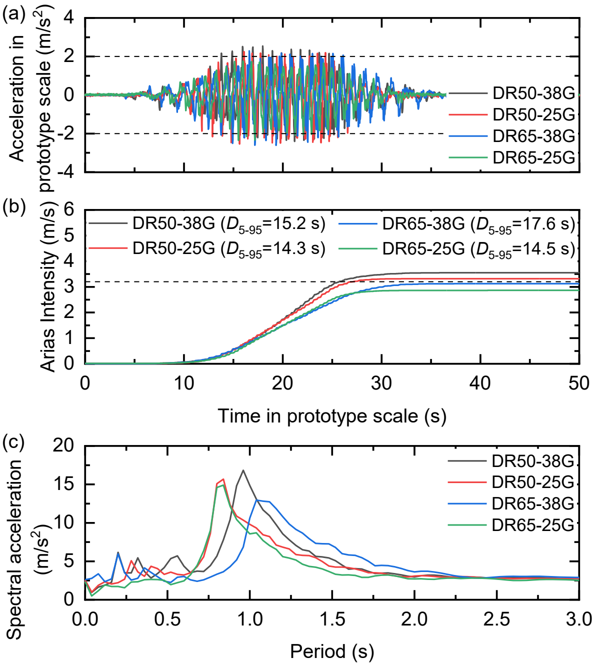

Figure 3. Input base motions; (a) acceleration, (b) Arias Intensity, (c) spectral acceleration.

3 RESULT AND DISCUSSION

3.1 Cone penetration resistance

Figure 4 shows the tip resistance profiles before (CPT#1) and after (CPT#2) shaking. Before shaking, the tip resistance increases with depth and tends to be higher at higher relative densities. The plots in the figure represent the tip resistance for D_r = 65% soil, calculated using the regression equation compiled by Carey et al. (2020) in LEAP-UCD-2017. Although the experimental results for D_r = 65% show some scatter between the two cases, it is noteworthy that they are generally consistent with the empirical values.

After shaking, no significant change in tip resistance is observed in the D_r = 65% cases. In contrast, both D_r = 50% cases show a distinct increase in tip resistance near the ground surface. At a depth of 0.5 m, the resistance after shaking increased from the initial values by a factor of 2.1 and 1.8 for DR50-38G and DR50-25G, respectively. This is likely due to the heaving of the foundation caused by the settlement of the dam body, as discussed in the next section.

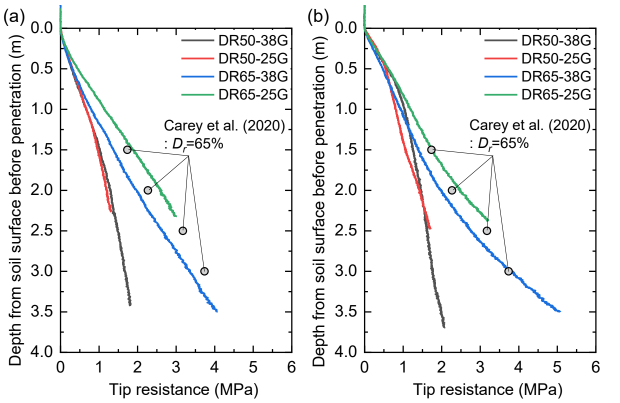

Figure 4. Profiles of measured penetration resistance; (a) before shaking motion (CPT#1), (b) after shaking motion (CPT#2).

3.2 Soil displacement

Figure 5 displays the soil displacement vectors obtained through PIV (Particle Image Velocimetry) analysis, superimposed on a photograph taken after the completion of shaking. To prioritize capturing the global deformation trend rather than localized precision, the PIV analysis was conducted using Flow-vec software (Library Co., Ltd.) with only two photographs: one from before and one after the shaking. By adopting this approach with a wide search window, it was possible to visualize the overall failure mechanism and displacement field of the embankment, even though some localized regions with extreme deformation did not reach a complete numerical solution. Since the g-level varies across cases, the displacement vectors are presented at the model scale for better clarity.

Table 2 shows the vertical displacements at the prototype scale determined from the PIV analysis. The reference points correspond to the locations shown in Figure 5: the crest, the ground surface, and the underground.

In the case of D_r = 50%, the base of the dam body underwent significant bowl-shaped deformation. The displacement vectors are uniform from the crest to the base of the dam, indicating that the volumetric compression of the dam body itself is small; thus, the settlement at the crest is approximately equal to the settlement of the foundation ground. Furthermore, the displacement vectors of the dam body exhibit minimal horizontal components, suggesting that the dam did not experience lateral stretching. Due to the settlement of the dam body, the foundation ground directly beneath it was pushed outward, resulting in heaving deformation outside the toes of the dam.

In the case of D_r = 65%, the settlement of the dam body is smaller compared to the D_r = 50% case. Diagonal displacement components are observed near the toes; this is because the bowl-shaped deformation at the base is less pronounced, causing the toes to displace slightly outward.

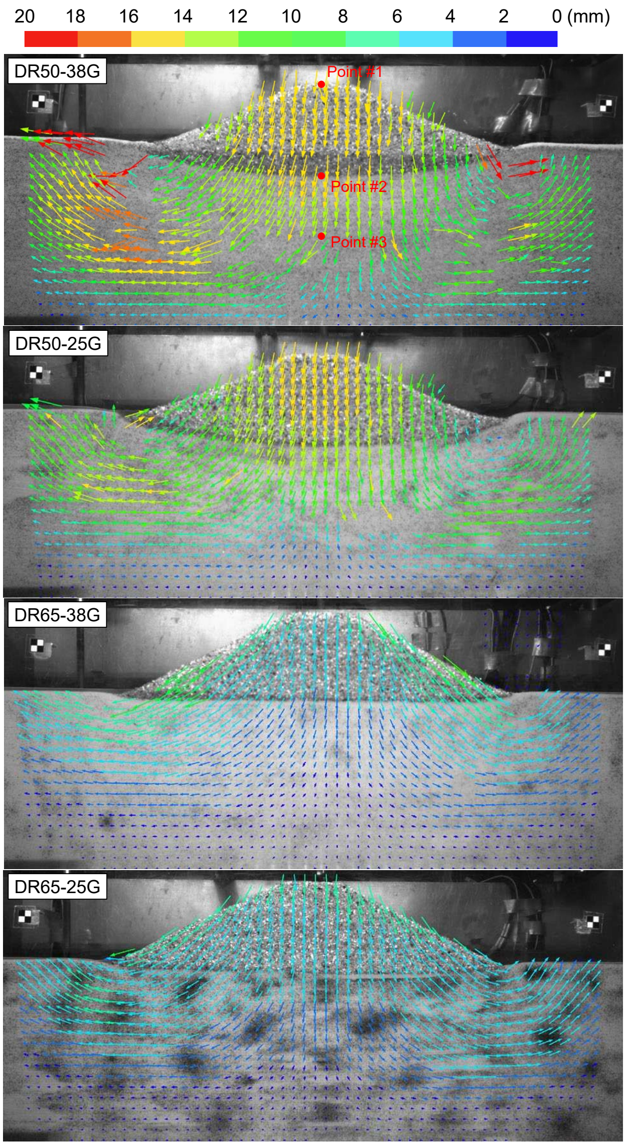

Figure 5. Displacement vectors on the side view.

A higher relative density tends to result in a shallower deformation zone and smaller heaving components outside the toes. However, the displacement vector distributions of DR50-38G and DR50-25G, as well as DR65-38G and DR65-25G, show good agreement despite their different g-levels. This indicates that the influence of g-levels on the model-scale deformation is minor, regardless of the relative density.

Table 2. Vertical displacements in prototype scale at the reference points obtained from PIV analysis.

Case ID	Point #1	Point #2	Point #3
DR50-38G	0.64	0.57	0.30
DR50-25G	0.37	0.36	0.29
DR65-38G	0.22	0.15	0.05
DR65-25G	0.16	0.11	0.05

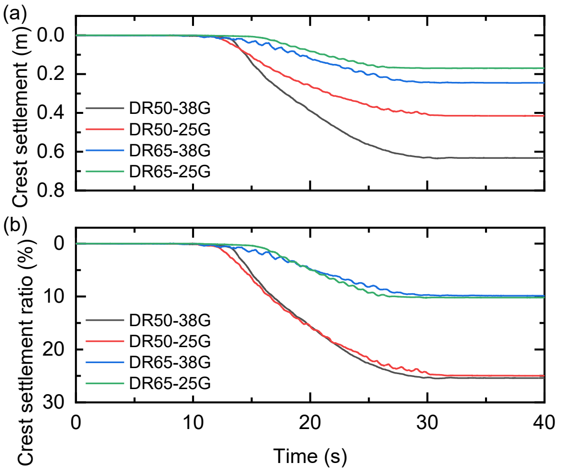

Figure 6. Time histories of; (a) crest settlement, (b) crest settlement ratio.

Figure 6 shows the time histories of the crest settlement and crest settlement ratio. With the pre-shaking state as the baseline, the settlement ratio is defined as a dimensionless quantity obtained by normalizing the settlement by the initial dam height.

Crest settlement began shortly after the start of shaking, coinciding generally with the rise in excess pore water pressure described later. Settlement progressed only during the shaking period, with no continued displacement observed after the shaking ended. In the D_r = 50% case, settlement begins earlier and the final settlement is larger. A comparison between the crest settlement at Point #1 determined by the PIV analysis (Table 2) and the final settlement shown in Figure 6 (a) reveals that they are in very close agreement.

It is noteworthy that when comparing cases with the same relative density but different g-levels, the time histories of the settlement ratio show very close agreement. As mentioned above, this suggests that within a g-level range of up to 1.5 times (38 g and 25 g) in the present study, the scale effect on the deformation of both the embankment and the foundation ground is not significant.

3.3 Acceleration response

Figure 7 shows the time history of acceleration response for the DR50-38G as a representative example. A0 is the acceleration measured on the shaking table. Directly beneath the dam body, a slight attenuation is observed in the acceleration at A1, whereas no such trend is seen at A2 and A3. At locations A4 through A6 near the toe of the slope, the acceleration begins to accumulate on the negative side from approximately 15 s; as shown in Figure 5, this suggests that the accelerometers tilted due to the displacement of the foundation. In the horizontal ground where A7 and A8 are embedded, the acceleration exhibits spikes at around 15 s followed by distinct attenuation, indicating the influence of liquefaction occurrence.

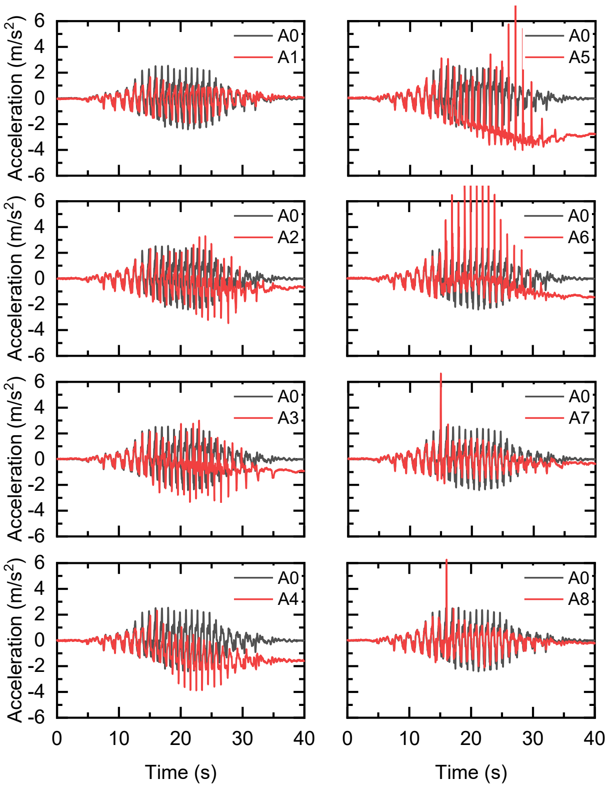

Figure 7. Acceleration in DR50-38G.

3.4 Pore pressure response

Figure 8 shows the time histories of the excess pore pressure ratio (r_u) for all cases. The r_u was calculated by dividing the excess pore pressure by the vertical effective stress, which accounts for the dam height at each sensor depth.

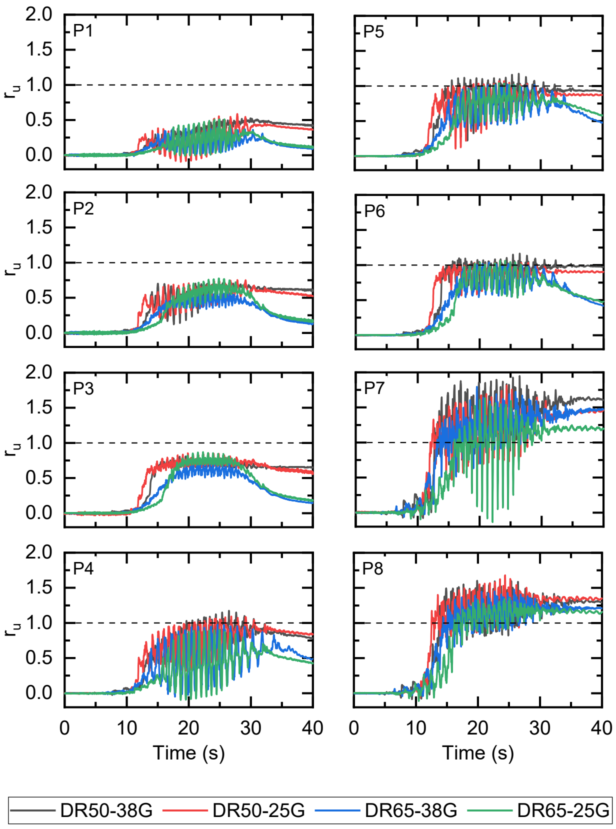

Figure 8. Excess pore pressure ratio.

The r_u shows similar behavior for each relative density, indicating high reproducibility of the results. Compared to the D_r = 50% cases, the D_r = 65% cases exhibit a slower rate of r_u increase, while the dissipation after the end of shaking is faster. Furthermore, a more pronounced drop in r_u is observed from P4 to P8 in the higher density case. These observations collectively reflect the influence of higher soil density.

In all cases, the r_u at P1–P3, located directly beneath the crest, remaine well below 1.0. In contrast, the r_u reach a maximum of approximately 1.0 at P4–P6 near the toe and exceed 1.0 at P7 and P8 in the horizontal ground section. Despite not reaching 1.0, the r_u at P1–P3 exhibit the characteristic behavior of liquefied ground by maintaining a constant high pressure. These spatial variations in the maximum r_u are attributed to differences in the horizontal stress state induced by the dam body and the horizontal constraint conditions. Beneath the crest, where lateral displacement is permitted and the vertical effective stress is large, the mean effective stress remained consistently lower than the vertical effective stress, preventing the excess pore pressure from reaching the initial vertical effective stress. On the other hand, in the sand near the toe and in the horizontal ground, the increase in horizontal stress due to the embankment load was dominant. This resulted in the mean effective stress exceeding the vertical effective stress, thereby allowing the excess pore pressure to surpass the initial vertical effective stress. These behaviors were consistent with the observations of previous centrifuge tests (Okamura et al., 2025).

Furthermore, focusing on the time-history waveforms, a distinct difference in oscillation characteristics was observed depending on the sensor location. As noted in the response of P5 for the DR65-38G and DR65-25G cases, the r_u exhibits significantly larger oscillations compared to the relatively smooth response at P2. This difference can be attributed to the influence of initial static shear stress. At the toe and slope locations (P4–P6), the soil elements are subjected to a non-zero static shear stress, causing the stress path to approach the phase transformation line asymmetrically. This leads to cyclic mobility behavior, which manifests as the observed large oscillations in the pore pressure response. In contrast, the soil beneath the crest (P1–P3) is in a more symmetric stress state with minimal initial shear stress, resulting in a more stable accumulation of r_u.

4 CONCLUSIONS

This paper presents the results of four centrifuge model tests conducted at Ehime University as part of the LEAP-Asia-2025 project. The experiments investigated the effects of relative density (D_r = 50% and 65%) and centrifugal acceleration (38 g and 25 g) on the deformation behaviour of a dam body constructed on a liquefiable foundation.

PIV analysis and settlement measurements using laser displacement transducers revealed that the crest settlement was highly dependent on the relative density. However, the normalized settlement ratio remained consistent regardless of the g-level, suggesting that the scale effect was minor for the g-level range used in this study (25–38 g).

Furthermore, while the r_u beneath the crest remained below 1.0 due to high vertical effective stress and lateral displacement, it reached or exceeded 1.0 near the toe and in the horizontal ground section. These variations highlight that the liquefaction response is primarily governed by the horizontal stress state and confinement conditions induced by the embankment load.

While this study focuses on the primary liquefaction behaviour, a detailed investigation of the seismic amplification characteristics using elastic response spectra remains a critical subject for future research and will be addressed in a subsequent study.

ACKNOWLEDGEMENTS

The authors are grateful for the support of Mr. Tamaoka of Ehime University in conducting the centrifuge tests.

REFERENCES

Carey, T.J., Gavras, A., Kutter, B.L. (2020). Comparison of LEAP-USD-2017 CPT results. *Model tests and numerical simulations of liquefaction and lateral spreading: LEAP-UCD-2017*, pp. 117–29. https://doi.org/10.1007/978-3-030-22818-7_6.

Kutter, B.L., Manzari, M., Zeghal, M. (2020). Preface. *Model tests and numerical simulations of liquefaction and lateral spreading: LEAP-UCD-2017*, https://doi.org/ 10.1007/978-3-030-22818-7

Ma, Q. (2025). LEAP-Asia-2025 V. 1.0 Model Specifications.

Okamura, M., Inoue, T. (2012). Preparation of fully saturated model for liquefaction study. *Int J Phys Model Geotech*, 12(1), pp. 39–46. https://doi.org/10.1680/ijpmg.2012.12.1.39

Okamura, M., Suyama, M., Ono, K. (2025). Effectiveness of sheet pile enclosure with drainage ability as liquefaction countermeasure for river levees, *Soils and Foundations*, 65, 101564. https://doi.org/10.1016/j.sandf.2024.101564

Ono, K., Okamura, M. (2024). Stability of sheet-pile wall in liquefiable soil: LEAP-2020 and LEAP-2022 centrifuge tests at Ehime University. *Soil Dynamics and Earthquake Engineering*, 182, 108743. https://doi.org/10.1016/j.soildyn.2024.108743

Wang, R., Liu, H., Kutter, B.L., Zhang, J.M. (2023). Influence of centrifuge test soil-container friction on seismic sheet-pile wall response in liquefiable deposit: insights from numerical simulations. *J of Geotech Geoenviron Eng*, 149(9), https://doi.org/10.1061/JGGEFK.GTENG-11064. 04023068-1–04023068-14.